

## Section 2

# PROGRESS IN LASER FUSION

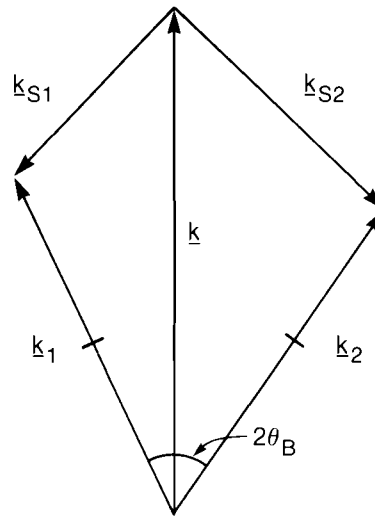
### 2.A Parametric Instabilities Driven by Two Pumps in Laser-Fusion Plasmas

Parametric instabilities of importance to laser-plasma interactions in laser-fusion experiments are usually analyzed assuming only one laser beam (pump) drives each instability. In actual experiments, however, multiple laser beams may overlap in a localized region of the fusion target corona, where parametric instabilities may be driven by more than one pump. In the simplest case, shown in Fig. 26.1, three-wave instabilities driven by one pump become five-wave instabilities driven by two pumps; the angle between the pumps is  $2\theta_B$ , the angle between the fixed positions of two illuminating beams. Five-wave parametric instabilities are the main subject of this article.

To summarize the results presented here, a homogeneous plasma model is first used to calculate growth rates and thresholds for five-wave Raman scattering and for two-plasmon decay. An inhomogeneous plasma slab with a linear density gradient is then considered. Heuristic arguments indicate that two pumps driving two-plasmon decay act independently, resulting in two inhomogeneous three-wave instabilities, instead of one five-wave process. Growth rates and thresholds for inhomogeneous five-wave Raman sidescattering are then calculated. Finally, a simple model is used to predict a spectral range of enhanced five-wave Raman sidescatter. A peak close to the one predicted is found in Raman spectra observed in six-beam, 351-nm OMEGA experiments.

#### Homogeneous Plasma Results

The growth rates and thresholds for five-wave parametric instabilities in a homogeneous plasma can be calculated by simple generalization



P497

Fig. 26.1  
Wave vector diagram for typical five-wave parametric instability. Two pumps  $k_1$  and  $k_2$  are at a fixed angle  $2\theta_B$ . The three daughter waves are  $k_1$ ,  $k_{s1}$ , and  $k_{s2}$ .

of the familiar calculations of three-wave instabilities.<sup>1</sup> The dispersion relation for five-wave Raman scattering producing two scattered electromagnetic waves, is, for example,

$$\begin{aligned}
 & (\omega_l^2 - \omega_p^2 - 3k_l^2 v_e^2) (\omega_s^2 - \omega_p^2 - k_{s1}^2 c^2) (\omega_s^2 - \omega_p^2 - k_{s2}^2 c^2) \\
 & = k_l^2 \omega_p^2 [ |v_1|^2 (\omega_s^2 - \omega_p^2 - k_{s2}^2 c^2) + |v_2|^2 (\omega_s^2 - \omega_p^2 - k_{s1}^2 c^2) ] \quad (1)
 \end{aligned}$$

Here  $\omega_l$  and  $k_l$  are the frequency and wave vector of the longitudinal or plasma wave;  $\omega_p$  is the plasma frequency;  $v_e = (T_e/m_e)^{1/2}$  is the electron thermal velocity;  $\omega_s = \omega_o - \omega_l$ , where  $\omega_o$  is the frequency of both pumps;  $k_{s1}$  and  $k_{s2}$  are the wave vectors of the scattered electromagnetic waves; and  $|v_1| = |v_2| = |v_o|$ , where  $v_o \equiv (-ie E_o/m_e \omega_o)$ , is the electron quiver velocity, taken to be the same for both pumps. To obtain Eq. (1), the beating of pump 1 or 2 with scattered wave 2 or 1, respectively, has been neglected. This approximation is good when, because of Bohm-Gross dispersion, the waves produced by these beat interactions do not satisfy the three-wave matching conditions; for typical experimental parameters<sup>2</sup> the frequency mismatch is large compared to the five-wave growth rate at perfect matching, and the approximation is well satisfied. No special coherence or phase relation between the two pumps is required to obtain Eq. (1), although each pump itself is assumed coherent. The five-wave vectors in Fig. 26.1 are assumed coplanar, with all electromagnetic wave polarizations perpendicular to their plane. This maximizes the growth rate of the instability. (If  $k_l$  makes an angle  $\alpha$  with respect to the plane defined by  $k_1$  and  $k_2$ , the growth rate is typically proportional to  $\cos \alpha$ .)

Solutions of Eq. (1) in various limits illustrate how five-wave parametric instability growth rates and thresholds differ from their three-wave counterparts. Consider Eq. (1), when one pump is perfectly matched to the plasma wave and corresponding electromagnetic wave. Write  $\omega_\ell = \omega_p + \delta\omega$ , and allow damping rates  $\nu_\ell, \nu_{s1}, \nu_{s2}$  (for collisional or Landau damping) and a frequency mismatch  $\Delta$  between the second pump and second scattered wave,  $\omega_o = \omega_p + (\omega_p^2 + k_{s2}^2 c^2)^{1/2} + \Delta$ , and take  $\delta\omega, \nu_\ell, \nu_{s1,2}, \Delta \ll \omega_p$ . Solutions of Eq. (1) are expressed in terms of the longitudinal wave vector at perfect matching, which, neglecting Bohm-Gross dispersion, is

$$\begin{aligned} k_\ell &= k_M(\omega_p, \theta) \\ &= k_o \left( \cos\theta + \left\{ \cos^2\theta + \frac{\left(\frac{\omega_p}{\omega_o}\right) \left[\left(\frac{\omega_p}{\omega_o}\right) - 2\right]}{\left[1 - \left(\frac{\omega_p}{\omega_o}\right)^2\right]} \right\}^{1/2} \right), \end{aligned} \quad (2)$$

where  $\theta$  is the angle between the perfectly matched pump and  $k_\ell$ .

Three-wave Raman results at perfect matching are recovered from Eq. (1) when  $\nu_2 = 0$ . The undamped growth rate becomes

$$\delta\omega \rightarrow i\gamma_1 \equiv \frac{i}{2} k_M |\nu_1| \left(\frac{\omega_p}{\omega_o - \omega_p}\right)^{1/2}, \quad (3)$$

while the threshold against damping becomes

$$\gamma_1^2 > \nu_\ell \nu_{s1}. \quad (4)$$

When  $\nu_2 \neq 0$ , the growth rate is maximized when both pumps are perfectly matched to their respective scattered waves,  $\Delta = 0$ . This is easily verified by treating Eq. (1) perturbatively, expanding  $\delta\omega$  in integral powers of  $\Delta$ . The maximum growth rate is then

$$\delta\omega \rightarrow i(\gamma_1^2 + \gamma_2^2)^{1/2} = i\sqrt{2}\gamma_1, \quad (5)$$

when  $\gamma_1 = \gamma_2$ . The ratio of five-wave to three-wave maximum Raman growth rates, assuming all pumps in both cases have the same intensity, is thus

$$\frac{\sqrt{2}k_M(\omega_p, \theta_B)}{k_M(\omega_p, 0)} \sim \sqrt{2} \cos\theta_B,$$

which is greater than 1 when  $\theta_B < \pi/4$ . In this estimate  $\theta = \theta_B$  is required for perfect matching to two pumps at a fixed angle of  $2\theta_B$ . In the one-pump case,  $\theta$  is unconstrained and Raman growth is maximized at backscattering. The five-wave Raman threshold against damping, at perfect matching, is found to be

$$\gamma_1^2 > (\nu_\ell \nu_s / 2) \quad (6)$$

for  $v_s = v_{s1} = v_{s2}$ . This is a factor of 2 less than the three-wave threshold in Eq. (4). When the mismatch  $\Delta$  is large compared to the growth rate, the matched pump acts essentially independently of the mismatched pump.

For two-plasmon decay, the ratio of five- to three-wave maximum growth rates is just  $\sqrt{2}$ , independent of angle. This result corresponds to the familiar independence of angle of the maximum growth rate for three-wave two-plasmon decay.<sup>3</sup> Thus, one of the plasma wave vectors in the five-wave two-plasmon decay bisects the pump wave vectors, lying at the intersection of the hyperbolas of maximum growth for the three-wave decays driven by each pump.

All the homogeneous five-wave processes considered here occur in the presence of a density ripple created by the beating of the two pump waves. This ripple has been neglected in the preceding results. Calculations including the ripple show that fractional changes in growth rates are of order  $(v_o/v_e)^2$ , small enough to justify this approximation.

### Results in a Plasma with a Linear Density Gradient

Consider now five-wave parametric instabilities driven by two pumps in a slab plasma with a linearly inhomogeneous density profile  $n(x) = n_o (1 + x/L)$ . The plasma is homogeneous in the  $y$  and  $z$  directions. For two-plasmon decay, the two-pump process appears to be suppressed under typical experimental conditions, and multiple pumps act independently, each driving three-wave decay. In the theory of inhomogeneous three-wave two-plasmon decay,<sup>4,5</sup> the growth rate is maximized on the hyperbola of maximum growth for the homogeneous instability. Moving off the hyperbola, the inhomogeneous growth rate falls off rapidly. Referring to Fig. 26.2, the maximum growth rate for the five-wave instability should occur when one of the three plasma daughter waves ( $k_A$ ) is at the intersection of the hyperbolas of maximum growth for the two pumps. Furthermore, when the parameter

$$\beta \equiv 1.41 T_{\text{keV}}^2 / I_{14} \lambda_\mu^2 \gg 1$$

(where  $T$  is the electron temperature in keV,  $I$  is the pump intensity in  $10^{14}$  W/cm<sup>2</sup>, and  $\lambda$  is the pump wavelength in microns) as for OMEGA experiments with 351-nm light, the one-pump growth rate is sharply peaked near the vertex of each hyperbola. When angles between laser-beam directions are significant, as in 6-beam or 24-beam spherical configurations, the intersection of the hyperbolas is far enough from the vertices that the growth rate is much smaller than the maximum or, typically, actually negative or damped. Thus, in Fig. 26.2, the growth rate for the three-wave process including  $k_2$ ,  $k'_p$ , and  $k_B$  is much larger than, or even has the opposite sign of, the growth rate for the three-wave process including  $k_2$ ,  $k_{p2}$ , and  $k_A$ . Since inhomogeneous two-pump thresholds and growth rates typically differ from one-pump results by factors of 2 and  $\sqrt{2}$  respectively, as for the Raman results obtained next, the two-pump two-plasmon decay should be suppressed.

Modifications of five-wave Raman scattering in inhomogeneous plasmas under realistic experimental conditions are far more significant

and interesting than for two-plasmon decay. Consider Raman side-scattering with two pumps; this process<sup>6,7</sup> is absolutely unstable in the radial direction, and thus dominant at densities below quarter critical. Since the pumps have equal wavelengths, side-scatter constrains them to lie symmetrically about the density gradient, as shown in Fig. 26.3. In general, the longitudinal wave vector  $k_z$  has an arbitrary transverse component  $k_{zy}$ . This process can be analyzed exactly as the three-wave process is in Ref. 7, where the method of analysis is explained in detail.

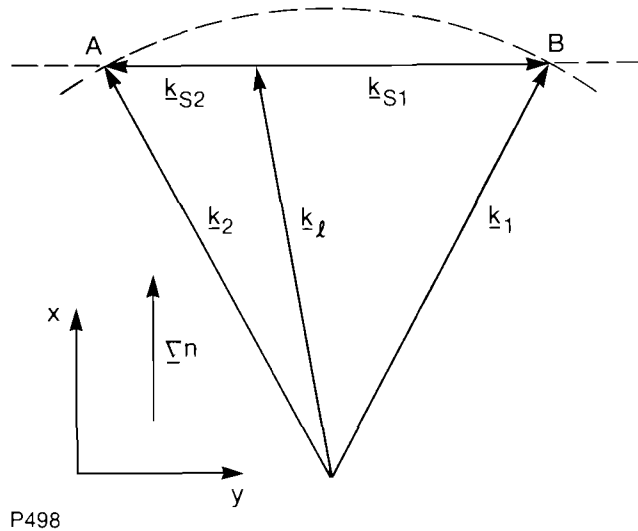


Fig. 26.2  
Five-wave two-plasmon decay in inhomogeneous plasma. Three-wave growth rates are sharply peaked on the hyperbolas of maximum growth. For  $\beta \equiv 1.41 (T_{kev}^2 / I_{14} \gamma_{\mu}^2) \gg 1$ , growth is further peaked near the vertices of the hyperbolas. Thus, the five-wave process, including decay wave  $k_A$ , is weakly growing or damped when the three-wave process, including decay wave  $k_B$ , is unstable.

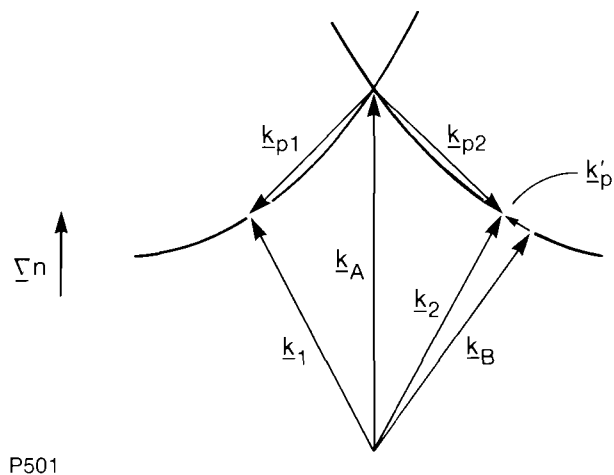


Fig. 26.3  
Two-pump inhomogeneous Raman side-scattering. Pumps must lie at the intersection of the line of side-scatter along  $\overline{AB}$ , and the circle  $|k_1| = |k_2| = |k_0|$ , along  $\overline{AB}$ .

In the homogeneous limit this analysis yields a dispersion relation of the form  $F_H = 0$ , where  $F_H$  is a fourth-order polynomial in  $k_{\ell y}^2$ . Thus,  $(\partial F_H / \partial k_{\ell y}) = 0$  at  $k_{\ell y} = 0$ , and the roots of  $F_H = 0$  occur in pairs that are reflections of each other through the origin of the complex  $k_{\ell y}$  plane, and are complex for  $|k_{\ell y}| \ll 1$ . Consequently, the instability is absolute in the  $y$  direction when  $k_{\ell y} = 0$ .<sup>8</sup> In the inhomogeneous case, it is evident from symmetry that the dispersion function  $D$  must have a double zero at  $k_{\ell y} = 0$  ( $\partial D / \partial k_{\ell y} = 0$  at  $k_{\ell y} = 0$ ), and the necessary condition for absolute instability in the  $y$  direction is satisfied. Furthermore, perfect matching to both pumps requires  $k_{\ell y} = 0$ . For these reasons, the strongest Raman sidescattering is found when  $k_{\ell y} = 0$ .

In this limit, growth rates and thresholds are computed as in Ref. 7. The dispersion relation is obtained from the Bohr-Sommerfeld eigenmode condition, applied after transforming in the  $x$  direction. It is solved by perturbing about the homogeneous limit, expanding in the small parameter  $(k_o L)^{-1}$ . As in the homogeneous case, the growth rate with two pumps is greater than that with one pump (with the same intensity as each of the two pumps) by a factor of  $\sqrt{2}$ ; the instability threshold for  $v_o^2$  is lower by a factor of 2 with two pumps than with one. These results are found by making a comparison with one pump whose angle of incidence in vacuum is  $\theta_B$ , and taking  $k_{\ell y} = 0$  at the matching density. However, since the one-pump sidescatter process is unconstrained, growth rates and thresholds comparable to the two-pump process can be found by varying the angle of incidence, as shown by Eq. (7) and Fig. 5 of Ref. 7.

An important property of the Raman sidescattering instability considered here is that, since it can satisfy perfect matching at only one density, it is spatially localized about that density. Since each density corresponds to a unique scattered wavelength in vacuum, this localization implies a peak in scattered wavelength. The width can be estimated by taking the first pump to be perfectly matched to the first scattered wave at each radius, and by computing the mismatch for the second pump. Using the homogeneous theory discussed previously as a guide, the two pumps should act independently when the mismatch becomes larger than the sidescattering growth rate  $\gamma \sim (v_o/c)\omega_{po}$ . Taking  $\Delta = 2\gamma$ , the spectral width  $\Delta\lambda_s$  can be estimated for typical parameters;  $(v_o/c) \sim 10^{-2}$ ,  $\theta_B \sim 40^\circ$ , as  $(\Delta\lambda_s/\lambda_{so}) \lesssim 0.02$  where  $\lambda_{so}$  is the scattered wavelength at perfect matching. This estimate suggests that two-pump Raman sidescattering will produce a spectral peak corresponding to the region of matching to both pumps.

### Comparison to Experiment

Since the spectrum of two-pump Raman sidescattering is so narrow in a slab model, the details of matching and spherical target-illumination geometry determine, in practice, the spectral peaks produced. The plasma frequency  $\omega_{pM}$ , at which matching to both pumps occurs, is found to be

$$\left(\frac{\omega_{pM}}{\omega_o}\right) = \frac{\cos^2 \theta_v}{2}, \quad (7)$$

where  $\theta_v$  is the vacuum angle between each pump and the density gradient. Figure 26.4 is a schematic diagram of a spherical target

illuminated by two tangentially focused beams. Each beam is a cone converging on the sphere. For simplicity, only rays in the plane defined by the beam axes are considered. Only symmetric pairs of rays, one from each beam, contribute to two-pump Raman sidescattering. When each ray in a pair makes an angle  $\alpha$  with its beam axis, the rays intersect at a geometric radius

$$r_G = \frac{D f \sin \alpha}{\sin(\theta_B - \alpha)} \quad (8)$$

where  $D$  is the target diameter, and  $f$  is the focal ratio of the lens. Refraction is neglected in obtaining Eq. (8), since, typically,  $(n/n_c) \sim 10^{-1}$  at  $r = r_G$  where  $n_c$  is the critical density. Note that  $\theta_v = (\theta - \alpha)$  in Fig. 26.4.

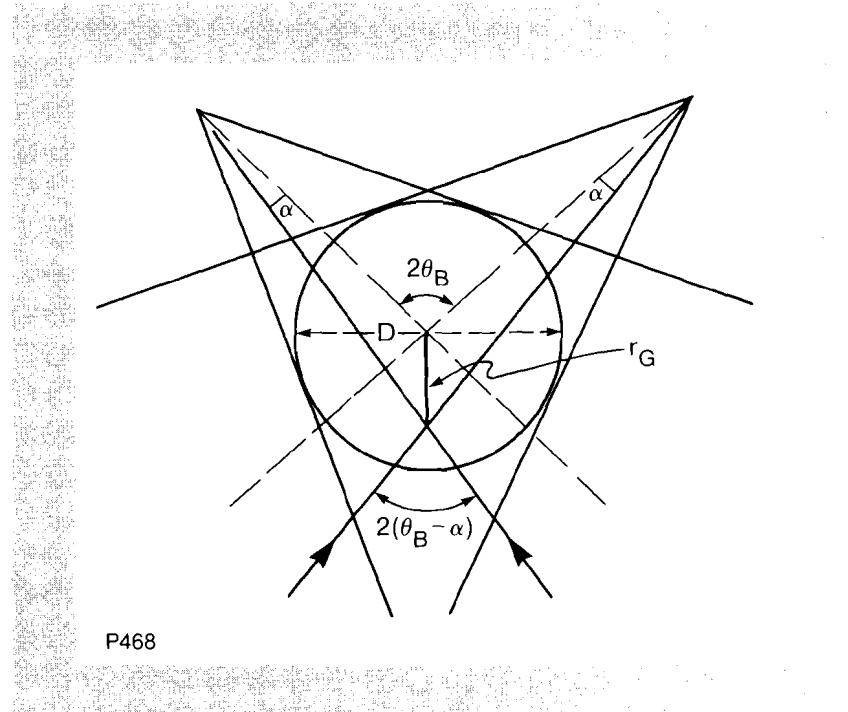


Fig. 26.4  
 Geometry of spherical target illuminated by two tangentially focused beams. Beam axes at angle  $2\theta_B$  are shown as dashed lines. Two incident rays, shown with arrows, intersect at radius  $r_G$ .

When the density at the geometric radius  $r_G$ , given by Eq. (8), coincides with the density required by Eq. (7) to satisfy matching, enhanced Raman scattering is predicted. Moving away from the region where these densities coincide, the scattering should be suppressed because, as discussed above, the instability is sharply peaked about the matching point. The wavelength of enhanced emission is most easily found using a graphics technique, as shown in Fig. 26.5. In this figure two different kinds of curves of the scattered wavelength in vacuum,  $\lambda_s$ , versus radius normalized to target diameter,  $(r/D)$ , are plotted. The first kind, curves A and A', are plots of the actual density profile. The density has been expressed as the scattered wavelength  $\lambda_s(r)$  that would be produced by Raman scattering at that density  $n(r)$  according to

$$\frac{\lambda_s(r)}{\lambda_o} = \frac{\omega_o}{\omega_s} = \left\{ 1 - \left[ \frac{n(r)}{n_c} \right]^{1/2} \right\}^{-1} \quad (9)$$

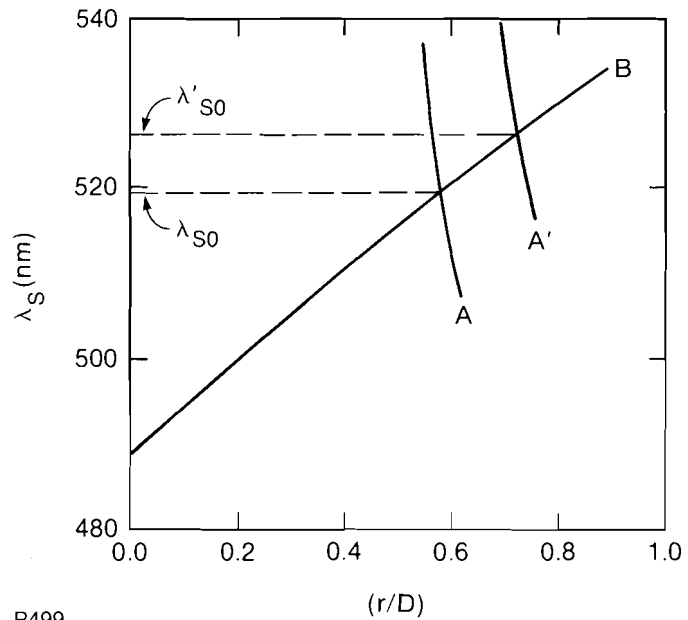


Fig. 26.5  
Determination of spectral region of enhanced two-pump Raman sidescattering. Curves A and A' are obtained from SAGE simulations of target density profiles for parameters described in text. Curve B is obtained from Eqs. (8) and (9), with  $\theta_B = 41.3^\circ$  and  $\alpha$  varying from 0 to  $\alpha_{MAX} = 7.13^\circ$ .

The second kind of curve, B, is a plot of  $\lambda_s(r)$  corresponding, via Eq. (9), to the density required for matching at each radius  $n_M$ . Curve B is obtained by considering all possible rays in the plane of the axes of two illuminating beams of half angular width  $\alpha_{MAX}$ . Thus, as  $\alpha$  is varied from 0 to  $\alpha_{MAX}$  in Eq. (8), all possible radii of intersection of pairs of rays in the beams are obtained. The corresponding density for each  $\alpha$  is obtained from Eq. (7), with  $(n_M/n_c)^{1/2} = (\omega_{DM}/\omega_o)$  and  $\theta_v = (\theta_B - \alpha)$ . The intersection of curves A (or A') and B corresponds to the radius where the actual density and the density required for perfect matching are equal. Raman scattering should then be peaked at the corresponding wavelength  $\lambda_{s0}$ . As parameters such as  $\theta_B$  and  $\alpha_{MAX}$  vary,  $\lambda_{s0}$  will shift, and may even cease to exist if the curves no longer intersect; the latter possibility is interpreted as the suppression of five-wave Raman scattering.

Analysis of experimentally observed Raman spectra requires realistic density profiles. Such profiles have been obtained from SAGE simulations.<sup>9</sup> Since these simulations follow the target implosion in time, a time-evolving density profile  $n(r,t)$  is obtained. If the variation of  $n(r,t)$  over the width of the pulse is plotted, curves such as A and A' in Fig. 26.5 are obtained. A corresponding spectral range of enhanced scattering, between  $\lambda_{s0}$  and  $\lambda'_{s0}$  in Fig. 26.5, is then predicted.

Spectra from OMEGA experiments with six 351-nm beams have been examined for the presence of two-pump Raman sidescattering, using the present model. Spectra were studied from shots with 82- $\mu$ m-diameter, solid CH spherical targets, illuminated by beams tangentially focused eight target radii beyond the target center, with a pulse width of 600 ps and an average intensity of  $1.8 \times 10^{15}$  W/cm<sup>2</sup>. In OMEGA

six-beam geometry the possible half angles between two adjacent beams are  $\theta_B = 41.3^\circ$  and  $48.7^\circ$ . Using the density profiles from SAGE simulations done with the same parameters as those of the experiments and a thermal flux limiter of 0.04, the curves in Fig. 26.5 are produced when  $\theta_B = 41.3^\circ$  and with  $\alpha_{MAX} = 7.13^\circ$ . For  $\theta_B = 48.7^\circ$ , similar curves do not intersect. Thus, a range of enhanced scattering is predicted between about 519 and 527 nm.

For comparison, two time-integrated Raman emission spectra from two different shots are overlaid in Fig. 26.6. Although the spectra differ greatly at most wavelengths, a peak between about 510 and 522 nm is seen to persist. In contrast, no such peak is evident in spectra from single beam experiments, such as those on GDL.<sup>10</sup> While the exact position and range of the peak differ somewhat from the values predicted by the two-pump Raman model, they are within the uncertainties of the experiment. The primary experimental uncertainty is in the pointing of the beams.<sup>11</sup> The axes of the beams in Fig. 26.4 can shift by as much as 20  $\mu\text{m}$  within this uncertainty – which, for an 80- $\mu\text{m}$ -diameter target, could (as seen from Fig. 26.5) account for 10-nm differences in the spectra. Considering, as well, the many approximations of the model, such as neglect of rays not in the plane of the beam axes, and the use of SAGE density profiles, the persistence of the peak provides preliminary evidence for the presence of two-pump Raman scattering.

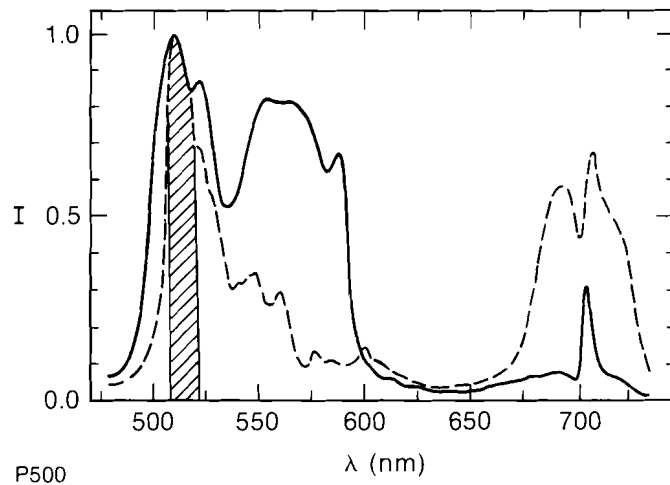


Fig. 26.6  
Raman spectra from six-beam, 351-nm OMEGA experiments. Spectra from two shots made under the same conditions are superimposed. Solid CH spherical targets of diameter 82  $\mu\text{m}$ , illuminated by beams tangentially focused at eight target radii, were used. Average intensity was  $1.8 \times 10^{15} \text{ W/cm}^2$  and pulse width was 600 ps. The cross-hatched region is the approximate peak common to both spectra.

### Discussion

The geometrical details of the theory clearly become more complicated when Raman sidescattering is driven by more than two pumps. Qualitatively, however, it is clear that additional peaks should be present in the resulting spectra. The results for two pumps suggest that for  $N$  pumps maximum growth rates could increase by a factor of  $\sqrt{N}$  and thresholds could decrease by a factor of  $N$ , compared to one pump with the same intensity as each of the  $N$ . Furthermore, the results

obtained here suggest that, in addition to the maxima associated with single-pump processes, the angular pattern of Raman scattering in multibeam experiments will have additional well-defined maxima, symmetric about the points where multiple beams symmetrically overlap. The heuristic discussion of inhomogeneous, two-pump, two-plasmon decay suggests that such additional maxima will not be found in the emission pattern associated with that process.

The results of this article imply that the interpretation of Raman spectra measured in multiple-beam direct-drive laser-fusion experiments requires a detailed understanding of Raman scattering driven by multiple pumps. Evidence indicating the occurrence of two-pump Raman scattering in blue, six-beam OMEGA experiments has been presented. Clearly, more experimental data from experiments with more beams, along with more detailed theory of multiple-pump instabilities in spherical geometry, will be required to test this interpretation.

#### ACKNOWLEDGMENT

This work was supported by the U.S. Department of Energy Office of Inertial Fusion under agreement No. DE-FC08-85DP40200 and by the Laser Fusion Feasibility Project at the Laboratory for Laser Energetics, which has the following sponsors: Empire State Electric Energy Research Corporation, General Electric Company, New York State Energy Research and Development Authority, Ontario Hydro, Southern California Edison Company, and the University of Rochester. Such support does not imply endorsement of the content by any of the above parties.

#### REFERENCES

1. J. F. Drake *et al.*, *Phys. Fluids* **17**, 778 (1974).
2. M. C. Richardson, R. S. Craxton, J. Delettrez, R. L. Keck, R. L. McCrory, W. Seka, and J. M. Soures, *Phys. Rev. Lett.* **54**, 1656 (1985).
3. C. S. Liu and P. K. Kaw, in *Advances in Plasma Physics*, edited by A. Simon and W. Thompson (Wiley, New York, 1976), Vol. 6, p. 114.
4. C. S. Liu and M. N. Rosenbluth, *Phys. Fluids* **19**, 967 (1976).
5. A. Simon, R. W. Short, E. A. Williams, and T. Dewandre, *Phys. Fluids* **26**, 3107 (1983).
6. C. S. Liu, M. N. Rosenbluth, and R. B. White, *Phys. Fluids* **17**, 1211 (1974).
7. B. B. Afeyan and E. A. Williams, *Phys. Fluids* **28**, 3397 (1985).
8. L. S. Hall and W. Heckrotte, *Phys. Rev.* **166**, 120 (1968).
9. R. S. Craxton and R. L. McCrory, Laboratory for Laser Energetics Report LLE-99 (1980).
10. K. Tanaka, L. M. Goldman, W. Seka, M. C. Richardson, J. M. Soures, and E. A. Williams, *Phys. Rev. Lett.* **48**, 1179 (1982).
11. F. Marshall (private communication).